BIOCHEMISTRY
including biophysical chemistry & molecular biology

Article

pubs.acs.org/biochemistry

Theoretical Study of the Catalytic Mechanism of E1 Subunit of Pyruvate Dehydrogenase Multienzyme Complex from *Bacillus stearothermophilus*

Xiang Sheng[†] and Yongjun Liu*[,†,‡]

[†]Key Laboratory of Theoretical and Computational Chemistry in Universities of Shandong, School of Chemistry and Chemical Engineering, Shandong University, Jinan, Shandong 250100, China

[‡]Northwest Institute of Plateau Biology, Chinese Academy of Sciences, Xining, Qinghai 810001, China

Supporting Information

ABSTRACT: Pyruvate dehydrogenase multienzyme complex (PDHc) is a member of a family of 2-oxo acid dehydrogenase (OADH) multienzyme complexes involved in several central points of oxidative metabolism, and the E1 subunit is the most important component in the entire PDHc catalytic system, which catalyzes the reversible transfer of an acetyl group from a pyruvate to the lipoyl group of E2 subunit lipoly domain. In this article, the catalytic mechanism of the E1 subunit has been systematically studied using density functional theory (DFT). Four possible pathways with different general acid/base catalysts in decarboxylation and reductive acylation processes were explored. Our calculation results indicate that the 4′-amino pyrimidine of ThDP and residue His128 are the most likely proton donors in the decarboxylation and reductive acylation processes, respectively. During the reaction, each C−C and C−S bond formation or cleavage process, except for the liberation of CO_2, is always accompanied by a proton transfer between the substrates and proton donors. The liberation of CO_2 is calculated to be the rate-limiting step for the overall reaction, with an energy barrier of 13.57 kcal/mol. The decarboxylation process is endothermic by 5.32 kcal/mol, whereas the reductive acylation process is exothermic with a value of 5.74 kcal/mol. The assignment of protonation states of the surrounding residues can greatly influence the reaction. Residues His128 and His271 play roles in positioning the first substrate pyruvate and second substrate lipoyl group, respectively.

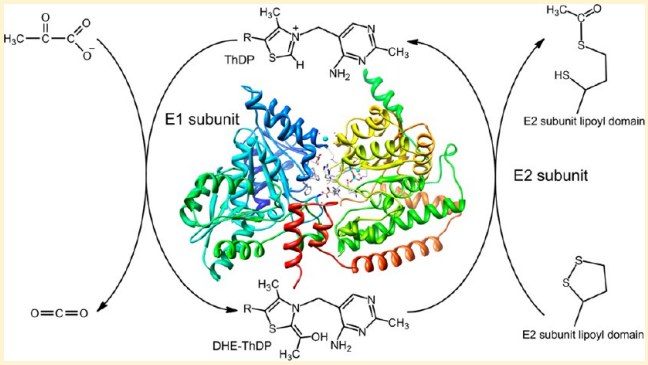

Pyruvate dehydrogenase multienzyme complex (PDHc) is nearly ubiquitous in organisms.[1−4] It is an important member of a family of 2-oxo acid dehydrogenase (OADH) multienzyme complexes, which are active at several central points of oxidative metabolism.[5] PDHc catalyzes the oxidative conversion of pyruvate and coenzyme A (CoA) into acetyl coenzyme A (acetyl-CoA) and CO_2 using NAD^+ as an oxidant in the following overall reaction 1:

$$\text{pyruvate} + \text{CoA} + \text{NAD}^+ \rightarrow \text{acetyl-CoA} + \text{CO}_2 + \text{NADH} + \text{H}^+ \quad (1)$$

Three different enzymatic components are required in the above challenging reaction (i.e., a thiamine diphosphate (ThDP)-dependent decarboxylase (EC1.2.4.1; E1), a lipoate-dependent acyltransferase (EC2.3.1.1; E2), and a flavin-dependent dihydrolipoyl dehydrogenase (EC 1.8.1.4; E3)).[6−9] The overall reaction can be divided into four steps. The first two steps are catalyzed by the E1 subunit, which involves the reversible transfer of a two-carbon fragment (acetyl group) from pyruvate to the lipoyl group of the E2 subunit's lipoly domain, as shown in Scheme 1. The third step is a transfer of the acetyl−lipoyl adduct to the acyltransferase domain of the E2 subunit, where the acetyl group further transfers to cofactor CoA. In the final step, the lipoyl domain of the E2 subunit visits the active site of the E3 subunit where the dithiolane ring of the lipoyl group is regenerated along with the reduction of NAD^+. Three components are assembled around a central core formed by multiple copies of the E2 subunit with either octahedral or icosahedral symmetry, depending on the organism.[10,11] The lipoyl domain of the E2 subunit is tethered to the peripheral

Scheme 1. Catalytic Reaction of PDH E1 Subunit

Received: May 7, 2013
Revised: October 9, 2013
Published: October 30, 2013

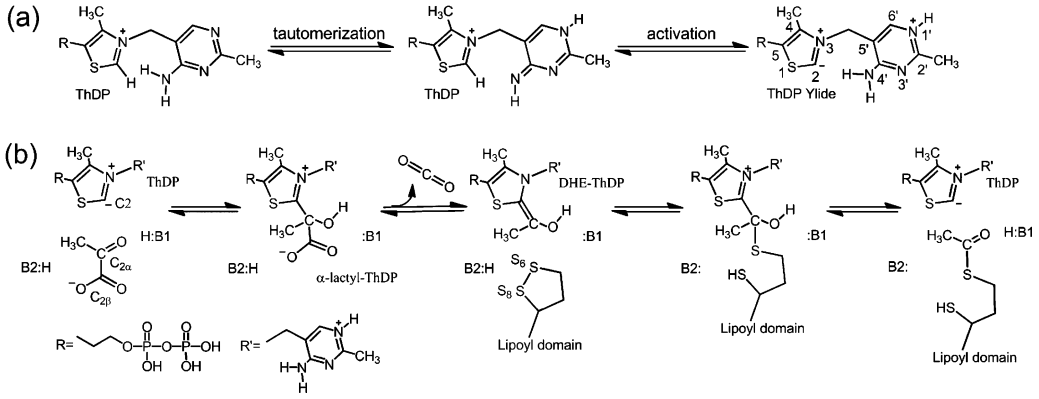

Figure 1. (a) Activation of ThDP and (b) the proposed catalytic mechanism of the PDHc E1 subunit.

subunit binding domain (PSBD) by means of a ∼50-residue flexible linker, which is highly mobile and can shuttle between all three subunits to enable communication among the catalytic active sites.[12,13]

The PDHc provides a link between glycolysis and the tricarboxylic acid (TCA) cycle. PDHc deficiency is one of the major genetic disorders leading to lactic acidosis[14,15] and is also found to be related to various types of brain damage and neurological symptoms, such as epilepsy[16] and infantile spasm.[17] The PDHc has been shown to be a therapeutic target for gene therapy.[18,19] More importantly, abundant evidence indicates that deficiency of the E1α subunit is the principal cause of PDHc deficiency.[20−22] Therefore, the E1 subunit is suggested to be the most important subunit in the entire multienzyme catalytic system, and understanding of the catalytic mechanism of the E1 subunit is enormously significant for regulating the activity of the PDHc and for designing novel drugs that have high efficiency.

The reaction catalyzed by the E1 subunit consists of the decarboxylation of pyruvate and the reductive acylation of the lipoyl group.[23,24] As shown in Figure 1, after activation of the cofactor ThDP, α-lactyl-ThDP is first formed by the attack of the C_2 carbanion of the ThDP ylide (active form of ThDP) on the $C_{2\alpha}$ atom of the substrate pyruvate. Then the scissile $C_{2\alpha}$−$C_{2\beta}$ bond of α-lactyl-ThDP is broken to generate the 1,2-dihydroxylethyl-ThDP (DHE-ThDP) carbanion/enamine intermediate, and the first product CO_2 is liberated. Subsequently, DHE-ThDP intermediate combines with the incoming second substrate lipoyl group of the E2 subunit lipoyl domain, which further undergoes a cleavage of the C_2−$C_{2\alpha}$ bond to release the final product (the acetyl−lipoyl adduct) and to regenerate the ThDP ylide. As shown in Figure 1, two general acid/base groups, namely, B1 and B2, are required for the whole reaction; B1 is responsible for the protonation of $C_{2\alpha}$ carbonyl of pyruvate, and B2 is functional to protonate one sulfur atom (S_8) of the lipoyl group.

Over the past decades, several crystal structures of the PDHc E1 subunit from different species, such as *Pyrobaculum aerophilum*,[25] *Escherichia coli*,[26] and *Bacillus stearothermophilus*,[23,27] have been solved. These 3D structures provided significant information for understanding the catalytic reaction. By comparing the obtained structures of the PDHc E1 subunit from different species, it was found that their active sites show high similarity. For example, all active sites of the PDHc E1 subunit are formed by α and β subunits and are located at the interfaces; like other ThDP-dependent enzymes, the cofactor ThDP maintains a so-called "V" configuration through surrounding hydrogen bonds and hydrophobic interactions, which is considered to be an essential prerequisite for catalysis.[28,29] Furthermore, the cofactors are almost completely buried, but the C2 atom is accessible from solution through the active-site clefts.

Until now, the reaction mechanism of PDHc E1,[24,30,31] the role of some key residues,[27,32−34] the communication among the active sites,[35,36] and some reaction intermediates[23,37,38] have been explored by experimental approaches. For example, Fries et al. carried out site-directed mutagenesis of a loop at the active site of the *B. stearothermophilus* E1 subunit and suggested that residue Arg267 is involved in the binding of the carboxyl group of the substrate and that other residues, including Tyr281, Asp276, and Arg282, have great influence on the decarboxylation and reductive acylation reactions.[32] Later, by examining the structure of the *E. coli* PDHc E1 subunit and yeast transketolase,[33] they proposed that a histidine residue is an important contributor for the reductive acylation. Further mutations of H271A and H128A indicated that His271 may be functional in the proton transfer and stabilization of the transition states during decarboxylation, whereas His128 may act as the proton donor in the subsequent reductive acylation.[23,24] In addition, Jordan et al. identified the various tautomeric forms of the 4′-aminopyrimidine ring using electronic spectroscopy and suggested the 1′,4′-imino tautomer of ThDP to be the first general acid/base group in the ThDP catalytic reactions.[39,40]

Although a rough picture of the catalytic mechanism of the PDHc E1 subunit has been obtained, as described in a review article,[29] open questions still remain. The detailed reaction pathway, the roles of pocket residues involved in proton transfer and stabilization of reaction intermediates and transition states, and the energetics of the whole catalytic cycle are still not fully understood. In addition, an explicit description of an enzymatic mechanism is crucial for exploring the biochemical role of enzymes and for designing novel drugs that have a high efficiency. Furthermore, some valuable information cannot be acquired by experimental data alone. Therefore, theoretical studies at the atomic level are required. However, in contrast to the extensive theoretical studies on the catalytic mechanism of some other ThDP-dependent enzyme, such as pyruvate decarboxylase (PDC),[41−43] pyruvate feredoxin oxidoreductase (PFOR),[44] acetohydroxyacid synthase (AHAS),[45−47] and transketolase (TK),[48] theoretical study of the reaction mechanism of the PDHc E1 subunit is still limited. Li et al. investigated the mechanism of ThDP activation and the decarboxylation reaction of the PDHc E1 subunit from *E. coli*

dx.doi.org/10.1021/bi400577f | *Biochemistry* 2013, 52, 8079−8093

by DFT methods.[49] Useful information was obtained; for example, two glutamate residues were considered to play essential roles in the ThDP ylide formation and in the orientation of the carboxyl of pyruvate. However, they suggested that after the decarboxylation of α-lactyl-ThDP the formed intermediate DHE-ThDP was subsequently protonated and was followed by the release of acetaldehyde. It is different from the generally accepted catalytic mechanism in which DHE-ThDP is bound with the lipoyl group of the E2 subunit lipoyl domain, which was then followed by the formation of final product, the acetyl–lipoyl adduct.[23,24,30,35] In their study, the reductive acylation of the second substrate lipoyl group was not included. In addition, the model used was based on a crystal structure without any substrate, which may not be a good model for the study of a catalytic reaction, and a more detailed study is necessary.

In this article, the catalytic mechanism of the PDHc E1 subunit has been studied using DFT methods[50,51] with cluster models, which has been widely applied in recent years in qualitatively elucidating enzymatic reaction mechanisms.[52−56] It is noted that combined quantum mechanics and molecular mechanics (QM/MM) methods have been increasingly developed in recent years for investigating the fundamental and practical problems of enzymology.[57−59] This should be the preferred approach for our study. However, the available QM/MM methods are usually more expensive than the simple QM calculation. Our aim is to solve the controversial question of mechanism and to understand qualitatively the transition-state structures and energetics of the catalytic reaction. Therefore, for such a complex system, the DFT method with cluster models was selected. The detailed energetic profile of the overall reaction as well as the structures of all of the intermediates and transition states along the reaction pathway are presented. The general acid/base groups and the roles of key pocket residues were determined.

COMPUTATIONAL METHODS

Cluster Models. The models used in this work are based on the recently obtained crystal structure of the PDHc E1 subunit from *B. stearothermophilus* (PDB code: 3DV0).[23] In this crystal structure, the PDHc E1 subunit is bound with a pyruvate and a ThDP analogue, 3-DEAZA-ThDP. The enzyme was recovered to its wild type by manually modifying the thiophene ring of 3-DEAZA-ThDP to thiazole ring. Each E1 subunit includes more than 20 000 atoms after adding hydrogen atoms. To improve computational efficiency, our model only contains the substrates, coenzyme ThDP, and some key residues, including His271 and His128, which are considered to act as the catalyst and/or to orientate substrate, Ile142, which forms a hydrogen bond with the 4′-amino group of ThDP, and Ile143, as shown in Figure 2. Residues Ile142, Ile143, and His271 and cofactor ThDP come from the same chain, and residue His128 comes from the neighboring chain. The second substrate lipoyl group, coenzyme, and all residues are truncated so that only important side chains or peptide backbones are included. During the optimizations, the truncated atoms and their H-link atoms were frozen to their crystallographic positions to prevent unrealistic movements of the groups involved in the model, and the fixed truncated atoms were marked with asterisks in the corresponding figures. One can see that only a few atoms were fixed in the model during the optimization, including the terminal carbon atoms and their H-link atoms of truncated residue His271, His128, Ile142, and Ile143 as well as the terminal carbon and oxygen atoms and their H-link atoms of truncated ThDP.

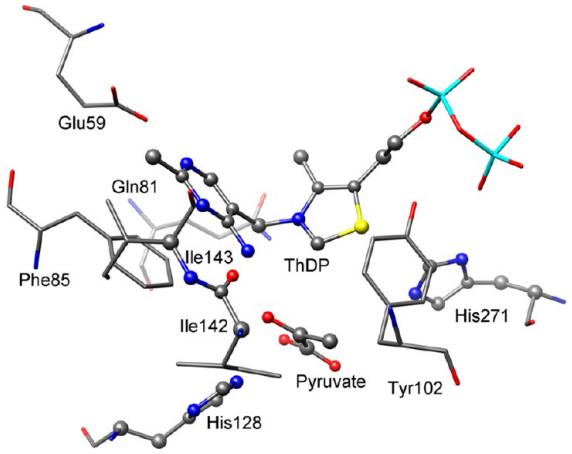

Figure 2. Crystal structure of the active site of the PDHc E1 subunit (PDB code: 3DV0) with substrate pyruvate and cofactor ThDP. The atoms used in our computational models are indicated by ball-and-stick.

Because the activation mechanism of ThDP has been extensively studied experimentally and computationally elsewhere,[41,49,60−62] our calculations start from a model in which ThDP has been activated (i.e., the proton at the C_2 carbon atom has been abstracted, and the ThDP ylide has been formed). It is well-known that a glutamate (Glu59 in PDHc E1 subunit from *B. stearothermophilus*) is significant in the catalytic reaction.[41,63,64] However, our test calculations (shown in Figure S1) indicated that this residue is less important in the reaction after the activation of ThDP. The crucial role of this glutamate is mainly in the activation process of ThDP, and our study focuses on the remaining steps; therefore, Glu59 was not included in our model.

Ionizable residues in the active sites exhibit significant influence on the substrate–enzyme interaction and catalytic reaction. To determine the protonation states of ionizable residues in the active site, preliminary calculations on the basis of mutational studies were first carried out. It is known that both His128 and His271 are located at the active site and that the lipoyl group is highly flexible; thus, both of the histidine residues are possible proton donors for the protonation of the lipoyl group. However, the complete inactivation of the H128A mutant and partial inactivation of H271A for the whole reaction in the experimental study strongly suggests that His128 is the sole proton donor in the reductive acylation process.[24] What is the reason that His271 cannot act as the proton donor in the reductive acylation process of the H128A-mutant-catalyzed reaction? One possibility is that the energy barrier of the rate-limiting step is greatly increased for the H128A mutant. We optimized the structures of the species involved in reductive acylation process catalyzed by the H128A (Path-H128A) mutant, and the obtained energy profile is shown in Figure S2 of the Supporting Information. From the energy profile, one can see that the highest energy barrier of this process is only 10.15 kcal/mol, which is still favorable. Thus, this possibility is excluded. Another possibility is that the residue His271 exists in its deprotonated state in the PDH E1 subunit. To examine this possibility, we employed the PROPKA 3.1 program[65,66] to estimate the pK_a value of the involved residues with the initial structure. The pK_a value of residue His271 was calculated to be

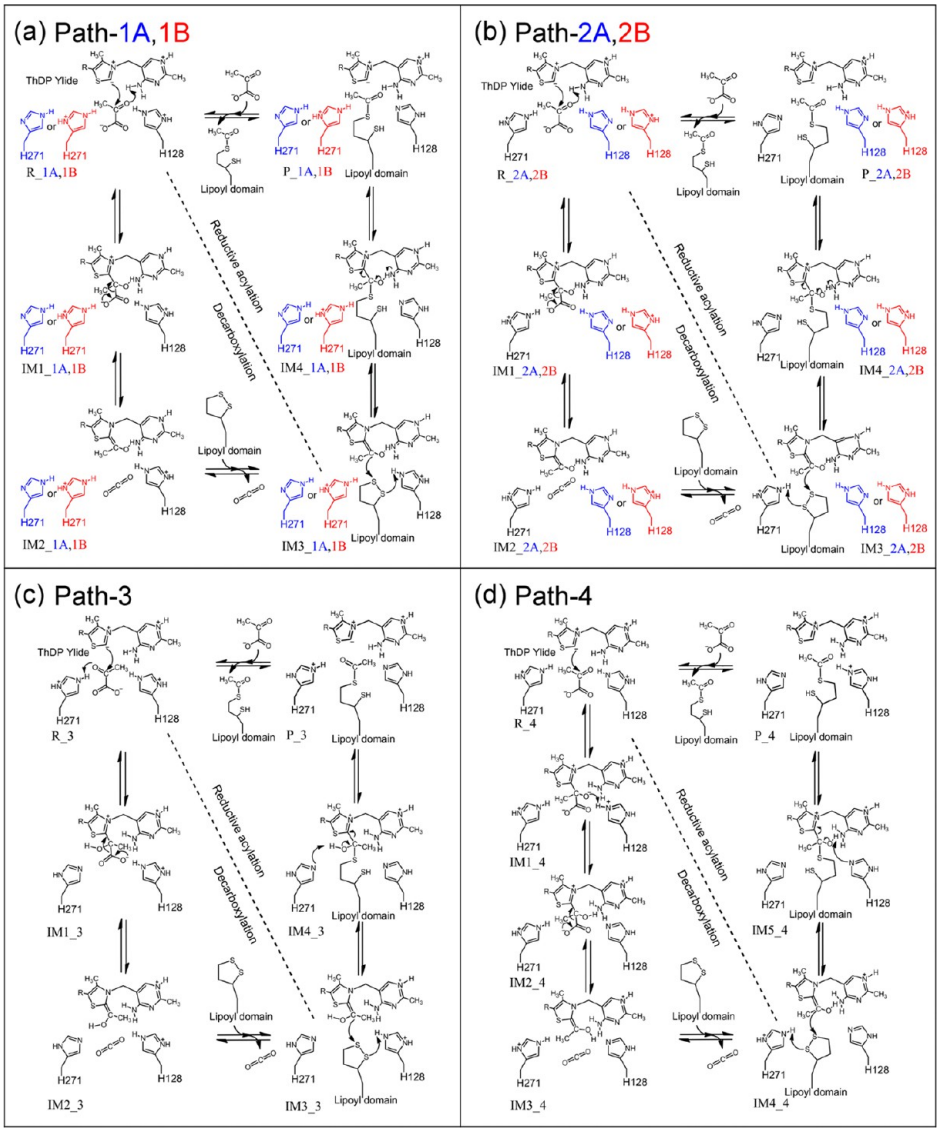

Figure 3. Four possible reaction pathways catalyzed by PDHc E1 subunit. (a) In Path-1, the 4′-amino of the ylide acts as B1, and residue His128 acts as B2 with His271 in a deprotonated state (Path-1A, in bule) or in a protonated state (Path-1B, in red). (b) In Path-2, the 4′-amino of ylide functions as B1, and residue His271 functions as B2 with His128 in a deprotonated state (Path-2A, in blue) or a protonated state (Path-2B, in red). (3) In Path-3, residues His271 and His128 are B1 and B2, respectively. (d) In Path-4, residue His128 serves as B1 and His271 serves as B2.

Table 1. Protonation States of Two Histidine Residues, Identities of Two General Acid/Base Groups, and Number of Atoms and Total Charge of Computational Models in Four Pathways

	protonation state of residues		general acid/base group			
	His128	His271	B1	B2	number of atoms	charges
Path-1A	protonated	deprotonated	4′-amino of ThDP	His128	87, 107[a]	+1, +1[b]
Path-1B	protonated	protonated	4′-amino of ThDP	His128	88, 108	+2, +2
Path-2A	deprotonated	protonated	4′-amino of ThDP	His271	87, 107	+1, +1
Path-2B	protonated	protonated	4′-amino of ThDP	His271	88, 108	+2, +2
Path-3	protonated	protonated	His271	His128	88, 108	+2, +2
Path-4	protonated	protonated	His128	His271	88, 108	+2, +2

[a]The two numbers represent the number of atoms from computational models in the decarboxylation and reductive acylation processes, respectively. [b]The two numbers represent the total charge from computational models in the decarboxylation and reductive acylation processes, respectively.

4.6, which is lower than the pH value of 7.0 under physiological conditions, indicating that residue His271 is in the deprotonated state. The pK_a value of residue His128 was calculated to be 7.4, meaning that it is in the protonated state. In addition, it has been reported that the active ThDP and α-lactyl-ThDP in the 2-oxo acid dehydrogenases may exist in their protonated forms.[40] Therefore, the protonated ylide form was adopted here.

Recent experimental study suggested that the 4′-amino pyrimidine of ylide is the general acid/base group (B1, as

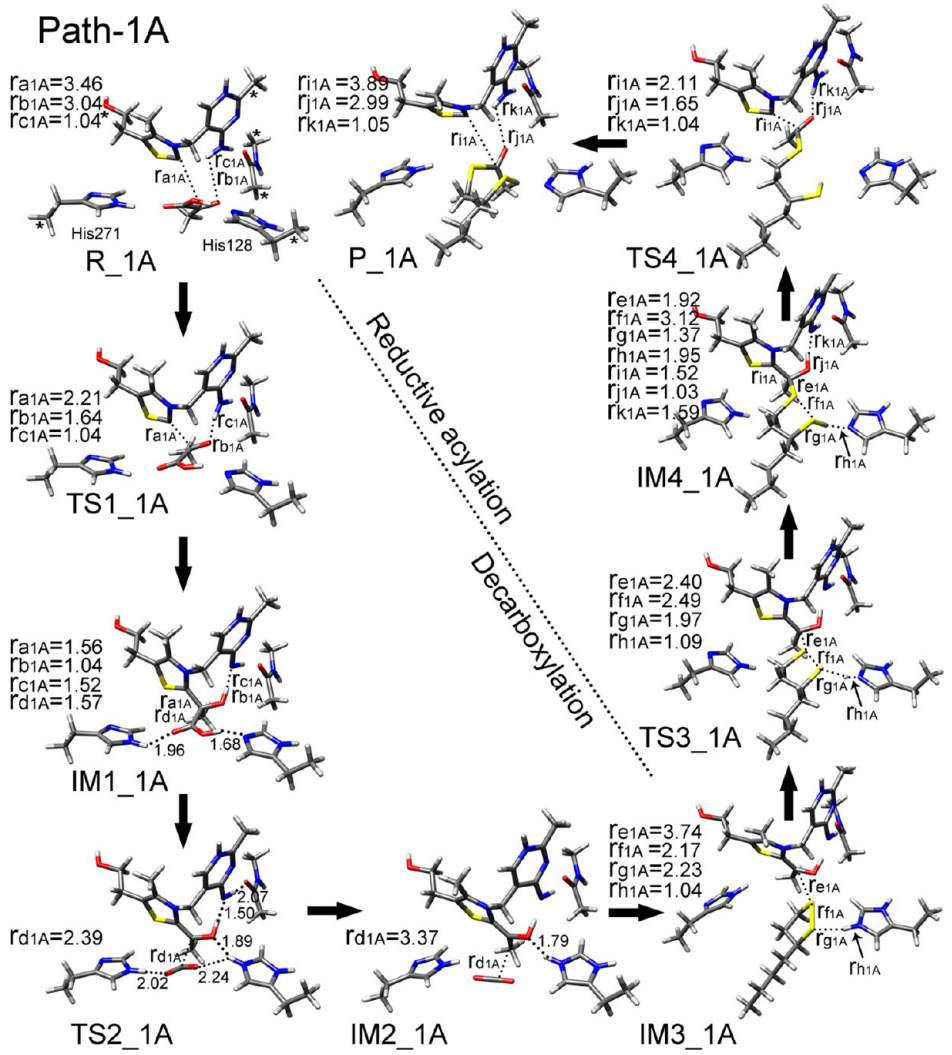

Figure 4. Optimized geometries for various species involved in Path-1A obtained at the B3LYP/6-31g(d,p) level. The key bond distances are shown in angstroms, and the fixed terminal atoms are labeled by asterisks in R_1A.

shown in Figure 1b) in the decarboxylation process and that residue H128 is the general acid/base (B2, as shown in Figure 1b) in the reductive acylation process.[23] In this pathway (named Path-1) and to investigate the influence of protonated states of surrounding residues on the catalytic reaction, residue His271 in the deprotonated (Path-1A) and protonated states (Path-1B) were both considered. Because the lipoyl group is highly flexible, it is also possible that residue His271 functions as the B2 if it is in the protonated state. Thus, the pathways with 4′-amino pyrimidine of the ylide acts as B1 and residue His271 acts as B2, where residue His128 in the deprotonated (Path-2A) and protonated states (Path-2B) were also studied here. Furthermore, in ref 24, residues His271 and His128 were suggested to be B1 and B2, respectively (Path-3), which was also included in this study. In addition, if both histidine residues exist in their protonated states, it is also possible that residues His128 serves as B1 and His271 serves as B2 (Path-4). The four possible pathways are shown in Figure 3. The protonation states of the two histidine residues, the identities of two general acid/base groups, the number of atoms, and total charge of computational models are summarized in Table 1.

Computational Details. All calculations presented here were carried out by means of the Gaussian 09 program package[67] using a hybrid density functional theory method. Geometrical structures were optimized at the B3LYP/6-31G(d,p) level of theory. To obtain more accurate energies, single-point calculations on the optimized structures were performed with the larger basis set 6-311++G(2d,2p), which includes diffuse functions and double polarization functions on each atom. To consider the effects of the rest of enzyme that were not included in our models on the energetics, we used the polarizable-continuum model (PCM)[68,69] to calculate the single-point energies at the 6-311++G(2d,2p) level for each species on the optimized geometries. In this model, the solvent is represented by a constant dielectric medium surrounding a cavity containing the solute. The empirical dielectric constant of the enzyme environment is chosen to be 4, which has been used in many studies.[70,71] Frequency calculations were performed with the 6-31G(d,p) basis set to obtain zero-point vibrational energies (ZPE) and to verify that all of the optimized geometries correspond to a local minimum that has no imaginary frequency or a saddle point that has only one imaginary frequency. Because some atoms were forced to their crystallographic positions during the structure optimization, a few small negative eigenvalues usually appear, typically in the order of 10 cm^{-1}. These frequencies do not contribute

dx.doi.org/10.1021/bi400577f | *Biochemistry* 2013, 52, 8079−8093

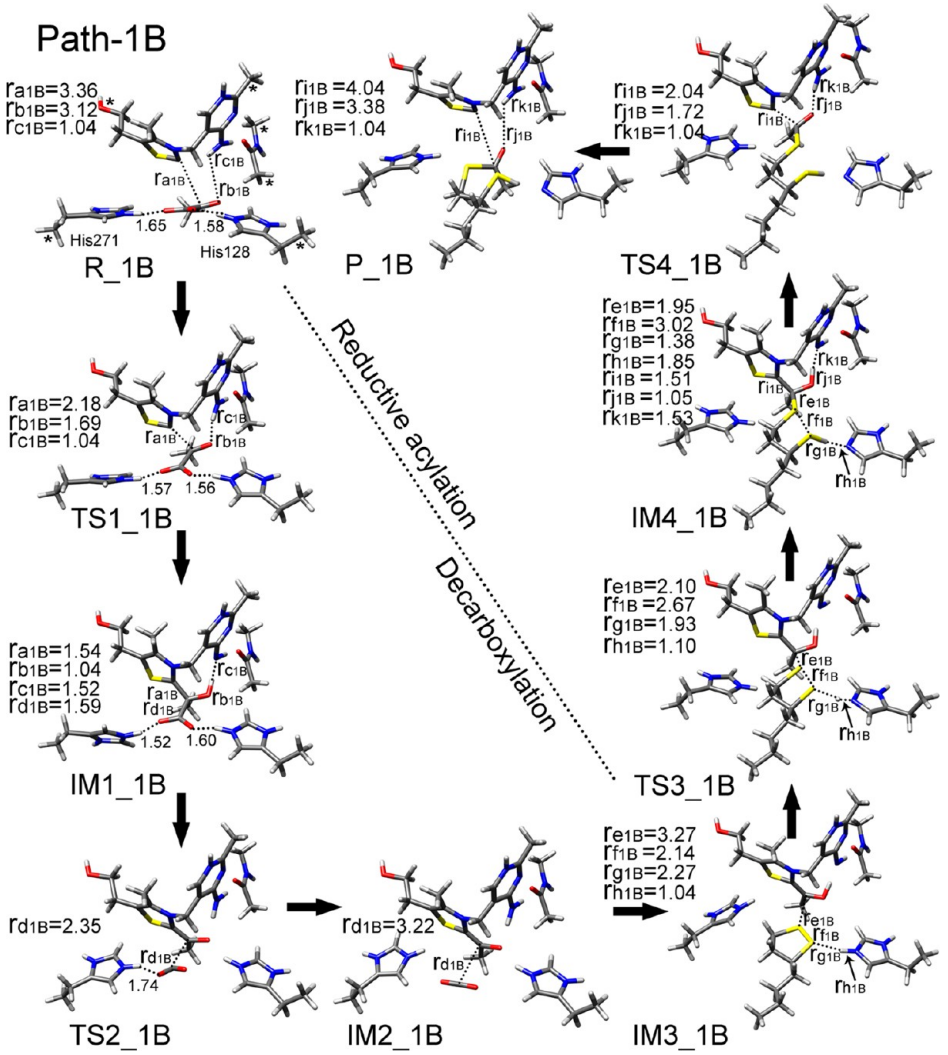

Figure 5. Optimized geometries for various species involved in Path-1B obtained at the B3LYP/6-31g(d,p) level. The key bond distances are shown in angstroms, and the fixed terminal atoms are labeled by asterisks in R_1B.

significantly to the zero-point energies and thus can be tolerated. In addition, freezing of some atoms reduces the freedom of a molecule, resulting in the model being slightly more rigid, and this can increase or decrease the energetics. However, it was demonstrated that no alterations on the conclusions were observed concerning the investigation of the catalytic mechanism caused by these effects. All of the transition states have been confirmed by intrinsic reaction coordinate (IRC) calculations.[72,73] The calculated IRC profiles for Path-1A are given in Figure S3 of the Supporting Information.

RESULTS AND DISCUSSION

Reaction Pathways. During the reaction, ThDP is well kept in its V-like conformation. The characteristic torsion angles Φ_T and Φ_P[74,75] for the orientation of the ThDP rings in all species are given in Table S1. To clearly elucidate the catalytic reaction, four pathways are discussed in the following sections. All of the reported energies are obtained in the solvent phase (PCM, ε = 4) at the B3LYP/6-311++g(2d,2p)//B3LYP/6-31g(d,p) level.

Path 1: ThDP as B1 and His128 as B2. The catalytic mechanism of Path-1 is shown in Figure 3a. First, the C_2 carbanion of the ThDP ylide attacks the $C_{2\alpha}$ atom of pyruvate, which is accompanied by a proton transfer from the 4′-amino of ThDP to the $C_{2\alpha}$ carbonyl of pyruvate, generating the α-lactyl-ThDP intermediate. Then, the DHE-ThDP intermediate is generated, and the first product CO_2 is liberated by the cleavage of the $C_{2\alpha}-C_{2\beta}$ bond. The following elementary reaction is the attack of the $C_{2\alpha}$ atom of DHE-ThDP on the S_6 atom of the lipoyl group coupled with the protonation of the S_8 atom by His128. After the formation of $C_{2\alpha}-S_6$ bond, the $C_2-C_{2\alpha}$ bond is broken to release the second product, the acetyl–lipoyl adduct, and to regenerate the ThDP ylide. We will first discuss the decarboxylation process and the reductive acylation process of Path-1A with His271 in the deprotonated state.

The optimized structures and key parameters of the reactant (R_1A represents the reactant in Path-1A, which is used similarly hereafter), transition states (TS1_1A and TS2_1A), and intermediates (IM1_1A and IM2_1A) in the decarboxylation process are shown in Figure 4. In the optimized structure of reactant R_1A, the proton of His128 has been transferred to the carbonyl group of pyruvate. Some hydrogen bonds (not shown in the figure) are formed between the substrate pyruvate, surrounding residues, and cofactor ThDP. The reactive C_2 atom of thiazolium ring positions a distance (r_{a1A}) of 3.46 Å from the $C_{2\alpha}$ of pyruvate. This optimized

dx.doi.org/10.1021/bi400577f | Biochemistry 2013, 52, 8079−8093

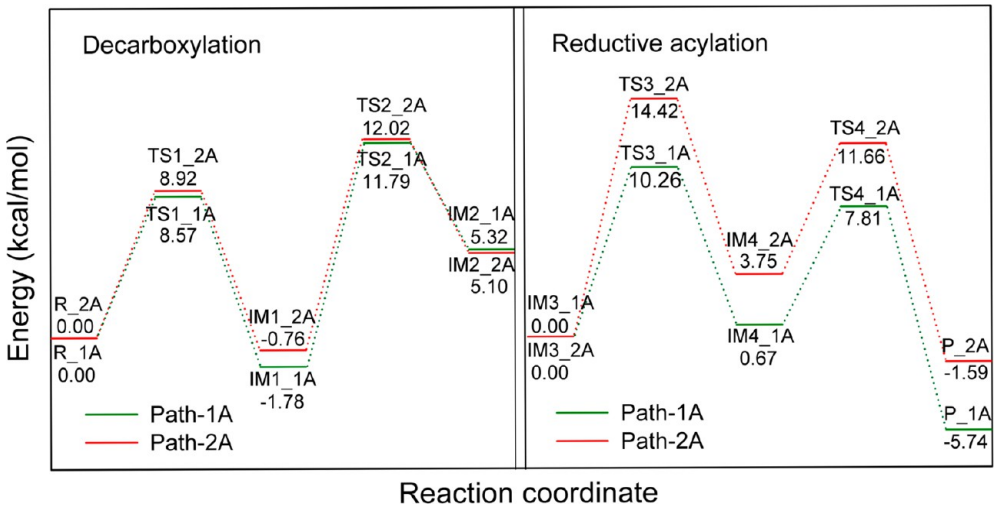

Figure 6. Energy profiles for Path-1A and Path-2A in the solvent phase (PCM, ε = 4). The ZPE-corrected relative energies (in kcal/mol) are obtained at the B3LYP/6-311++g(2d,2p)// B3LYP/6-31g(d,p) level. For comparison, we set the energies of both R_2A and R_1A to zero. In fact, R_2A is 0.36 kcal/mol higher in energy than R_1A, and IM3_2A is 3.63 kcal/mol lower in energy than IM3_1A.

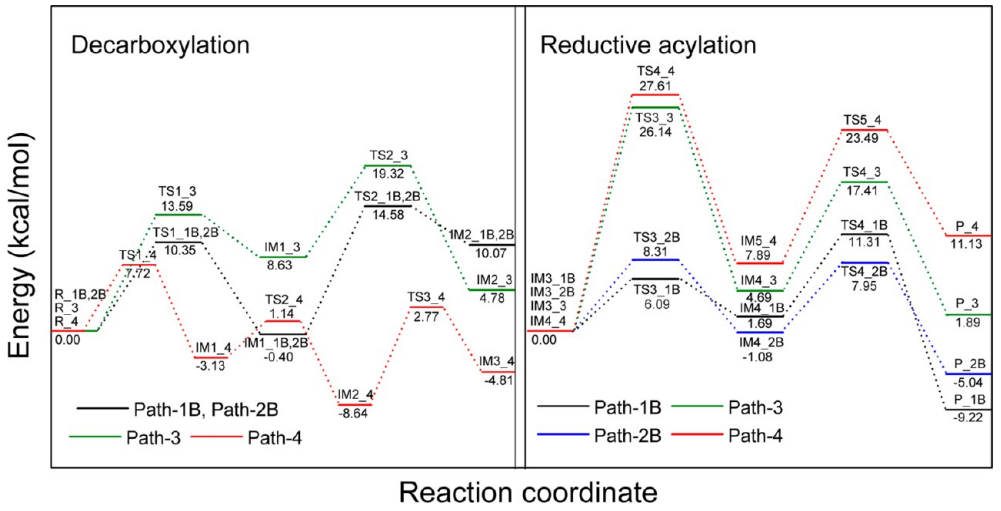

Figure 7. Energy profiles for Path-1B, Path-2B, Path-3, and Path-4 in the solvent phase (PCM, ε = 4). The ZPE-corrected relative energies (in kcal/mol) are obtained at the B3LYP/6-311++g(2d,2p)// B3LYP/6-31g(d,p) level. Because Path-1B and Path-2B correspond to the same decarboxylation process, they share an identical energy profile; however, IM3_2B is more stable than IM3_1B by 7.13 kcal/mol. In path-3 and path-4, R_3 and R_4 are 1.52 and 6.97 kcal/mol higher in energy than R_1B, and IM3_3 and IM4_4 are more stable than IM3_1B by 20.59 and 22.13 kcal/mol, respectively.

structure is favorable for the covalent addition of pyruvate. From R_1A to TS1_1A, r_{a1A} and r_{b1A} are shortened to 2.21 and 1.64 Å, respectively, whereas the length of the N−H bond of the 4′-amino of ThDP (r_{c1A}) is still 1.04 Å, indicating that the proton transfer has not started, whereas the C−N bond is on the way to be broken. Downstream from TS1_1A to IM1_1A, r_{a1A} and r_{b1A} change to 1.56 and 1.04 Å, respectively, indicating the completion of the ligation of the C_2−$C_{2\alpha}$ bond and proton transfer. Therefore, it can be concluded that this elementary reaction occurs in a concerted asynchronous mechanism and that the linkage of the C−C bond occurs prior to proton transfer. It can be seen from IM1_1A that two oxygen atoms of the carboxyl group of α-lactyl-ThDP form two hydrogen bonds with residues His128 and His271, respectively. Thus, these two residues may play important roles in the following decarboxylation. During the formation of CO_2, the hydrogen bond between the carboxyl group and His128 is disrupted, whereas the other hydrogen bond between the carboxyl group and His271 is maintained. Instead, His128 forms a hydrogen bond with the $C_{2\alpha}$ hydroxyl oxygen atom, as evidenced by the O(DHE-ThDP)−H(His128) distance of 1.79 Å in IM2_1A.

The optimized structures and key parameters of the intermediates, transition states. and product in the reductive acylation process of Path-1A are also shown in Figure 4. In IM3_1A, the hydrogen atom attached to nitrogen atoms of His128 interacts with the S_8 atom of the lipoyl group. From IM3_1A to TS3_1A, the distance between the $C_{2\alpha}$ atom of DHE-ThDP and the S_6 atom of the lipoyl group (r_{e1A}) are shortened to 2.40 Å from 3.74 Å. Meanwhile, the S_6−S_8 bond of the lipoyl group is broken with a change of distance (r_{f1A}) from 2.17 to 2.49 Å. In the intermediate IM4_1A, the $C_{2\alpha}$−S_6 bond is formed, and proton transfer is completed. One can see that the ligation of the $C_{2\alpha}$−S_6 bond occurs prior to proton transfer in this step. In the last step of the reaction from IM4_1A to P_1A via TS4_1A, the C_2−$C_{2\alpha}$ bond is broken with the distance between the two carbon atoms (r_{i1A})

dx.doi.org/10.1021/bi400577f | Biochemistry 2013, 52, 8079−8093

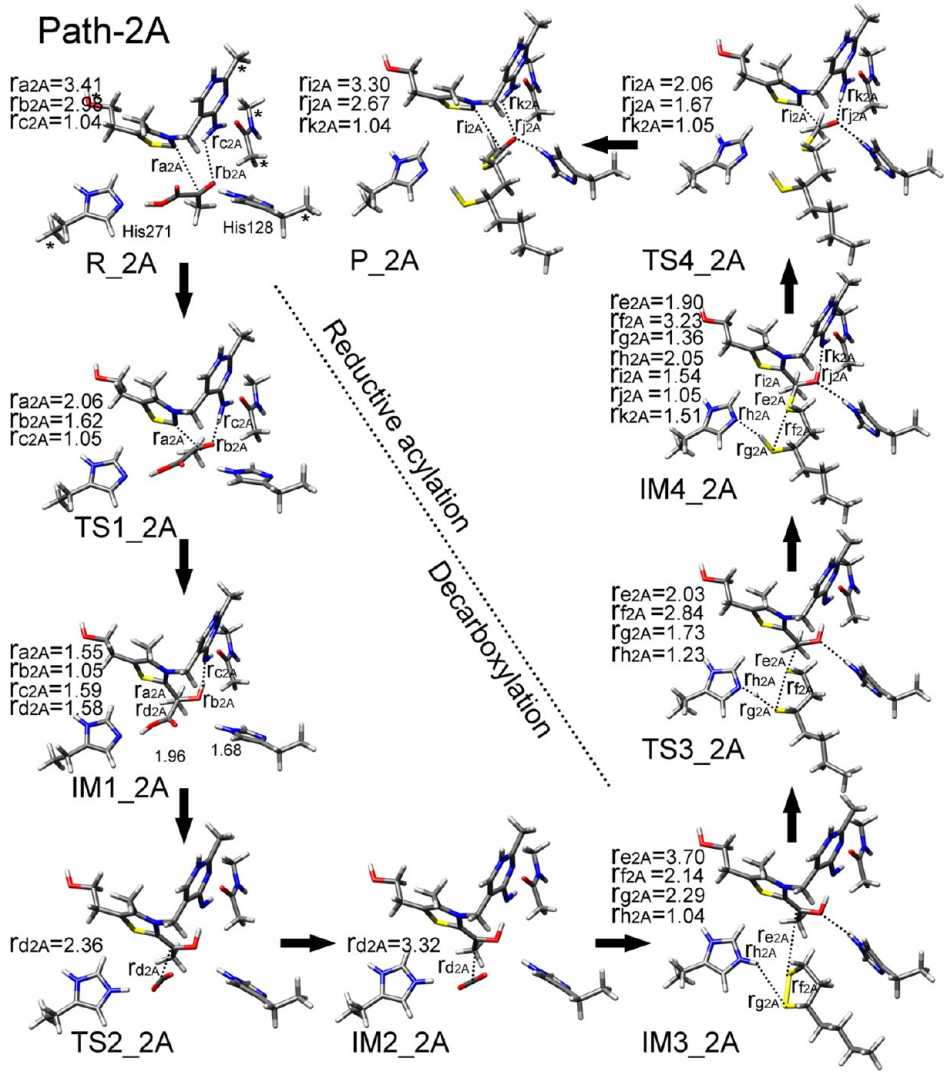

Figure 8. Optimized geometries for various species involved in Path-2A obtained at the B3LYP/6-31g(d,p) level. The key bond distances are shown in angstroms, and the fixed terminal atoms are labeled by asterisks in R_2A.

changing from 1.52 to 3.89 Å via 2.11 Å. Simultaneously, the hydrogen atom of the $C_{2\alpha}$ hydroxyl transfers to the 4′-amino of the thiazolium ring. The distance between the hydrogen atom of the $C_{2\alpha}$ hydroxyl and the nitrogen atom of the 4′-amino of the thiazolium ring (r_{k1A}) is 1.59, 1.04, and 1.05 Å in IM4_1A, TS4_1A, and P_1A, respectively, indicating the proton transfer occurs prior to the cleavage of the $C_2-C_{2\alpha}$ bond.

To investigate the influence of the protonated state of residue His271 on the reaction, Path-1B with His271 in the protonated state was also studied. The optimized structures and key parameters of all species involved in this pathway are shown in Figure 5. It can be seen that the structures of the species in this pathway are not significantly different from those in Path-1A. However, in Path-1B, there was no proton transfer from His128 to the carbonyl group of pyruvate during the optimization of the reactant. This may be due to the fact that the deprotonated carbonyl group of pyruvate can be greatly stabilized by the two protonated histidine residues.

The energy profiles of Path-1A and Path-1B are shown in Figures 6 and 7, respectively. From Path-1A, one can see that the formation of IM1_1A is calculated to be slightly exothermic by 1.78 kcal/mol with an energy barrier of 8.57 kcal/mol. The subsequent CO_2-liberation process corresponds to largest energy barrier of 13.57 kcal/mol in this pathway. In addition, α-lactyl-ThDP is relatively stable in the reaction, and the relative energy of IM2_1A is 7.10 kcal/mol higher than that of IM1_1A, meaning that the reaction will stop at the first step and that IM1_1A will be obtained if the reductive acylation process could not occur, which is consistent with the theoretical and experimental results of another ThDP-dependent enzyme, TK.[48,76,77] In the reductive acylation process, the calculated energy barrier of the ligation of the $C_{2\alpha}-S_6$ bond and the break of the $C_2-C_{2\alpha}$ bond are 10.26 and 7.14 kcal/mol, respectively. Earlier experimental studies suggested that the catalyzed reaction of the PDHc E1 subunit determines the overall rate of the whole PDHc reaction.[78−80] Here, we further confirm that the liberation of CO_2 is the rate-limiting step for the overall activity of the PDHc E1 subunit. In the study of another ThDP-dependent enzyme, PDC,[42] this step was also proved to be rate-limiting. In addition, the decarboxylation process is endothermic by 5.32 kcal/mol, whereas the reductive acylation process is exothermic with a value of 5.74 kcal/mol.

In Path-1B, the energy barriers of the formation of IM1_1B and IM2_1B is 10.35 and 14.98 kcal/mol, respectively, which are both are a little higher than that of Path-1A. However, in the following reductive acylation process, the ligation of the

dx.doi.org/10.1021/bi400577f | *Biochemistry* 2013, 52, 8079−8093

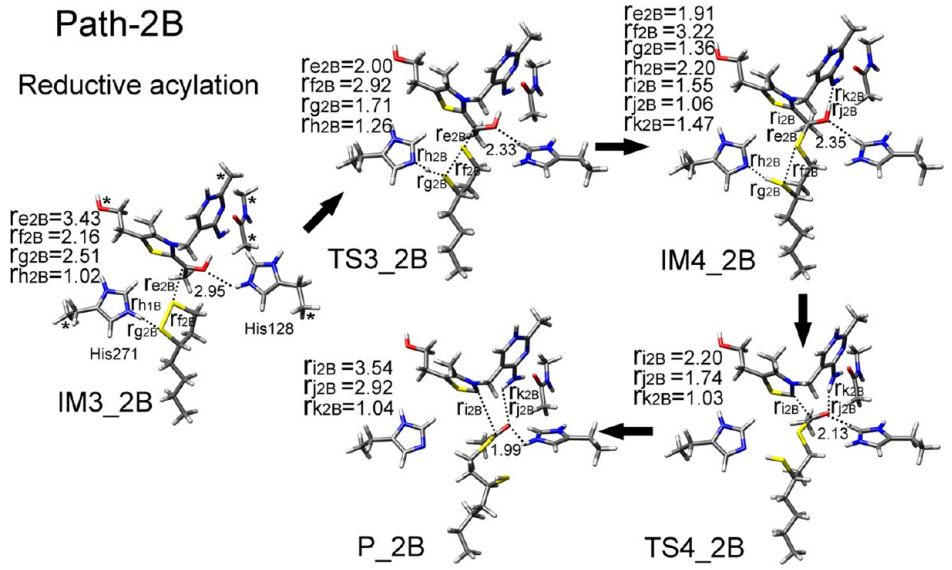

Figure 9. Optimized geometries for various species involved in the reductive acylation process of Path-2B obtained at the B3LYP/6-31g(d,p) level. The key bond distances are shown in angstroms, and the fixed terminal atoms are labeled by asterisks in IM3_2B.

$C_{2\alpha}$−S_6 bond is calculated to be 6.09 kcal/mol, which requires less energy than that of Path-1A. These barrier reductions are possibly due to the different charge distribution in the species of the two pathways. The protonation of residue His128 can greatly stabilize the structure of TS3_1B. Thus, we can conclude that the protonation of surrounding residues can influence the reaction greatly. As the energy barrier of the rate-limiting step in Path-1B is only 1.41 kcal/mol higher than that of Path-1A, it is also possible for the reaction to proceed via Path-1B. However, from the above discussion, we conclude that protonating residue His271 is difficult. Thus, the more favorable pathway is Path-1A. In addition, the entropy changes in all pathways are given in Table S2. The results indicate that the entropy effect only slightly influences the energies and cannot change the reaction pathways.

To examine the effect of the protein's electrostatic surroundings on the energy barriers, we also calculated the single-point energies in the gas phase and in water (PCM, dielectric constant ε = 80) for each species on the optimized geometries. These two energy profiles for Path-1A are shown in Figure S4. Compared with the energy profile in the surrounding enzyme, clear differences can be observed in the energy barriers of every step. Therefore, the enzyme environment can influence this enzymatic reaction. The same effects were found in the other pathways.

Path 2: ThDP as B1 and His271 as B2. In above Path-1B, both His128 and His271 are in their protonated states. It is also possible for residue His271 to function as B2 because the lipoyl group is highly flexible. Thus, the pathway in which the 4′-amino pyrimidine of the ylide acts as B1 and residue His271 as B2 with residue His128 in deprotonated (Path-2A) and protonated states (Path-2B) was also studied here. The only difference between Path-1B and Path-2B is the identity of the general acid/base that protonates the second substrate lipoyl group. Therefore, Path-1B and Path-2B share the same decarboxylation process.

The optimized structures and key parameters of all species in Path-2A and in the reductive acylation process of Path-2B are shown in Figures 8 and 9, respectively. The details of Path-2 is similar to that of Path-1 (i.e., the formation of the C_2−$C_{2\alpha}$ bond and proton transfer from the 4′-amino to the $C_{2\alpha}$ carbonyl oxygen of pyruvate also occur in a concerted asynchronous mechanism, and the proton transfer occurs later than the formation of the C_2−$C_{2\alpha}$ bond). In the following reductive acylation process and similar to Path-1, both the formation of the C_2−S_6 bond and the cleavage of the C_2−$C_{2\alpha}$ bond are accompanied by a proton transfer in a concerted asynchronous manner. However, clear structural difference can be found between IM3_2A and IM3_2B of Path-2 and IM3_1A and IM3_1B of Path-1 in the moiety of dithiolane and in residue His128. In IM3 of Path-1, residue His128 interacts with the S_8 atom of dithiolane by a hydrogen bond, meaning dithiolane locates in a favorable position for the protonation of the S_8 atom by His128. However, in IM3 (IM3_2A and IM3_2B) of Path-2, His128 forms a hydrogen bond with the $C_{2\alpha}$ hydroxyl oxygen atom, and the orientation of dithiolane is changed to facilitate proton transfer from His271 to the S_8 atom.

The energy profiles of Path-2A and Path-2B are shown in Figures 6 and 7, respectively. In the decarboxylation process, the calculated energy barriers for the formation of two intermediates IM1 and IM2 in Path-2A are 1.43 and 2.20 kcal/mol lower than those of Path-2B, respectively. Although in the reductive acylation process, the energy barriers of the formation of intermediates IM4 and product P in Path-2A are 6.11 and 1.12 kcal/mol higher than those in Path-2B, respectively. Thus, the protonation state of His128 influences the elementary reactions of the reductive acylation process moreso than those of the decarboxylation process. The reason may be that in the later process His128 forms strong hydrogen bond with the $C_{2\alpha}$ hydroxyl oxygen atom, which is bonded with the reactive $C_{2\alpha}$ atom directly. In Path-2A, the rate-limiting step is the ligation of the C_2−S_6 bond, with an energy barrier of 14.42 kcal/mol. In Path-2B, the liberation of CO_2 is calculated to be the rate-limiting step, with an energy barrier of 14.98 kcal/mol. The energy barriers of the limiting steps of both Path-2A and Path-2B are slightly higher than that of Path-1A. In addition, our calculations also reveal that R_2A is only 0.36 kcal/mol higher than R_1A. Considering that the energy profiles of decarboxylation of Path-1A and Path-2A are very

dx.doi.org/10.1021/bi400577f | *Biochemistry* 2013, 52, 8079−8093

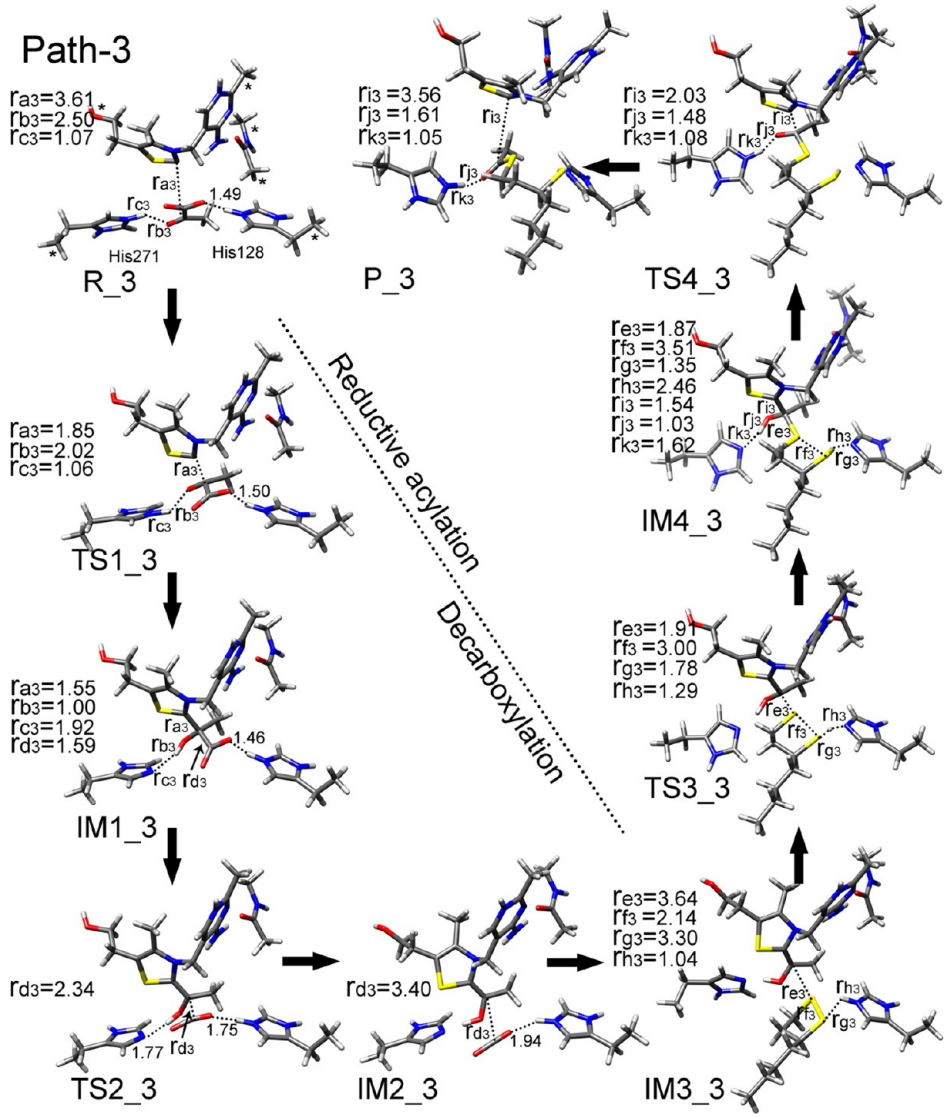

Figure 10. Optimized geometries for various species involved in the overall Path-3 catalytic cycle obtained at the B3LYP/6-31g(d,p) level. The key bond distances are shown in angstroms, and the fixed terminal atoms are labeled by asterisks in R_3.

similar, we concluded that the different protonation states of His128 and His271 have minor influence on the decarboxylation of the substrate. In the reductive acylation process, IM3_2A is calculated to be 3.63 kcal/mol more stable than IM3_1A. However, Path-2A corresponds to the larger energy barrier in this process. Furthermore, residue His271 is difficult to protonate. Thus, the pathway will proceed in Path-1A. In addition, we can also conclude that the protonation of surrounding residues can greatly influence the catalytic reaction.

Path-3: His271 as B1 and His128 as B2. In the crystal structure used in our study, the first substrate pyruvate is located in the same position as in Path-1 and Path-2. However, the orientation of the pyruvate was not definitively assigned using electron density maps.[23] The pyruvate can also exist in a conformation in which the $C_{2\alpha}$ carbonyl oxygen atom is hydrogen-bonded with His271. Furthermore, residue His271 was proposed to be a proton donor in the decarboxylation process in earlier studies.[24] Thus, the pathway with protonated His271 as B1 and protonated His128 as B2 (Path-3) is also considered, and the catalytic mechanism is shown in Figure 3c.

The optimized structures and key parameters of the reactant, transition states, intermediates, and product in Path-3 are shown in Figure 10. In reactant R_3, pyruvate is stabilized by some hydrogen bonds, one of which is formed by the $C_{2\alpha}$ carbonyl of pyruvate and by the imidazole ring of His271 with a distance of 2.50 Å, which is crucial for proton transfer. During the ligation of the $C_2-C_{2\alpha}$ and $C_{2\alpha}-S_6$ bonds in the decarboxylation process and the cleavage of $C_2-C_{2\alpha}$ in the reductive acylation process, proton transfer also occurs in a concerted but asynchronous manner. The hydrogen bond between the carboxyl group and His128 is well kept in the whole decarboxylation process, which may play a role in stabilizing the transition states and intermediates.

From the energy profile of Path-3 (Figure 7), we can see that the formation of the $C_{2\alpha}-S_6$ bond is the most energy-demanding reaction. The calculated energy barrier of this step is 26.14 kcal/mol, which is much higher than that of the earlier-discussed pathways. Thus, the reaction would not proceed via Path-3. Compared with the optimized structures of the transition states in Path-1A, the increase of the energy barriers can be explained from their structures. For instance, in the

dx.doi.org/10.1021/bi400577f | *Biochemistry* 2013, 52, 8079−8093

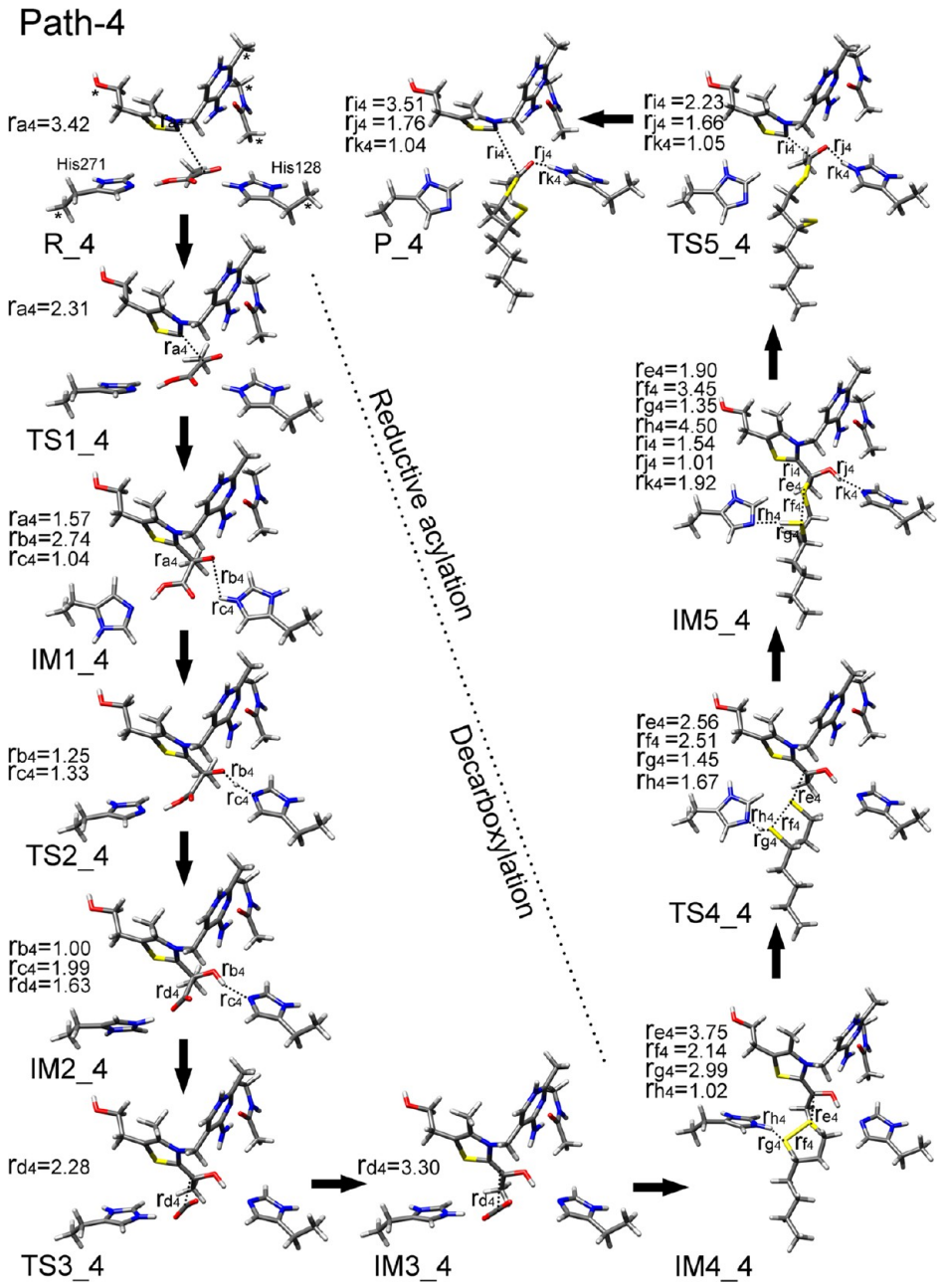

Figure 11. Optimized geometries for various species involved in Path-4 obtained at the B3LYP/6-31g(d,p) level. The key bond distances are shown in angstroms, and the fixed terminal atoms are labeled by asterisks in R_4.

transition-state structures of the liberation of CO_2 in Path-1A and Path-3, several hydrogen bonds are observed in both species (as shown in TS2_1A and TS2_3 in Figures 4 and 10). However, in TS2_1A, ThDP, Ile142, His128, and His271 form five hydrogen bonds, which can greatly stabilize the transition state and reduce the energy barrier.

Path-4: His128 as B1 and His271 as B2. In addition to the above pathways, the pathway (Path-4) with His128 as B1 and His271 as B2 was also studied. The optimized structures of all involved species are shown in Figure 11. Different from the reactants in the above pathways is that the R_4 residue His128 forms a hydrogen bond with the $C_{2\alpha}$ carbonyl oxygen of pyruvate instead of the carboxylic oxygen, which provides a necessary condition for proton transfer from His128 to pyruvate. After completion of the proton transfer, the deprotonated His128 is always hydrogen bonded to the $C_{2\alpha}$ hydroxyl group. Similar to other pathways, the ligation of the $C_{2\alpha}-S_6$ bond and cleavage of the $C_2-C_{2\alpha}$ bond are also companied by proton transfer in a concerted but asynchronous manner. However, different from the decarboxylation process in other pathways, the ligation of the $C_2-C_{2\alpha}$ bond and the proton transfer proceed in a stepwise manner. The energy profile of Path-4 is shown in Figure 7. For comparison, the relative energies of different pathway were also calculated. R_3 and R_4 are higher than R_1B in energy by 1.52 and 6.97 kcal/mol, and IM3_2B, IM3_3, and IM4_4 are 7.13, 20.59, and 22.13 kcal/mol more stable than IM3_1B. In the decarboxylation process, Path-4 corresponds to the lowest energy barrier. However, in the reductive acylation process, the energy barriers of Path-4 are high. In particularly, the ligation of the

dx.doi.org/10.1021/bi400577f | *Biochemistry* 2013, 52, 8079−8093

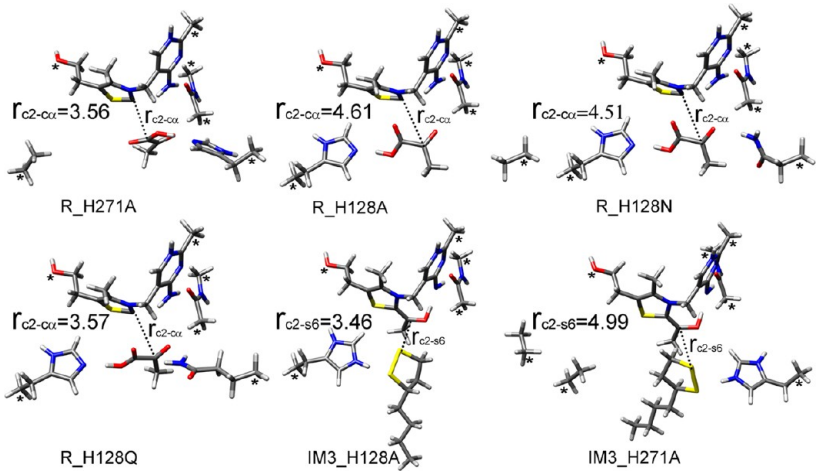

Figure 12. Optimized geometries for various mutants bound with pyruvate (R_H271A, R_H128A, R_H128N, and R_H128Q) and mutants bound with the lipoyl group of the E2 subunit lipoyl domain (IM3_H128A and R_H271A). The key bond distances are shown in angstroms, and the fixed terminal atoms are labeled by asterisks.

lipoyl group and DHE-ThDP corresponds to an energy barrier of 27.61 kcal/mol, indicating that Path-4 is unfavorable in energy.

Roles of Some Key Residues. Site-directed mutation is an effective tool to identify the roles of residues in substrate recognition, transition-state stabilization, conformational changes of active-site loops, and general acid/base functionality. Several mutational studies on the PDH E1 subunit have been carried out,[23,24,31] including H128A, H128N, H128Q, and H271A. Valuable information on the roles of residues H271 and H128 has been obtained, as mentioned above. To understand further the roles of these two residues, we optimized the structures of four pyruvate-bound mutants, namely, R_H271A, R_H128A, R_H128N, and R_H128Q as well as two lipoyl-bound mutants, IM3_H128A and IM3_H271A. Optimized geometries of all mutants are shown in Figure 12. In reactant R_1A of Path-1A for the wild-type enzyme, the distance between the C_2 atom of ThDP and the $C_{2\alpha}$ atom of pyruvate is 3.46 Å. However, in mutants H128A and H128N, these distances ($r_{c2-c\alpha}$ for all structures here) changed to 4.61 and 4.51 Å, indicating an unfavorable position of pyruvate for the reaction. In contrast, $r_{c2-c\alpha}$ only slightly changes to 3.56 Å in the H271A mutant and to 3.57 Å when H128 was substituted by glutamine (which still forms a hydrogen bond with the substrate). Thus, our calculations proved that residue H128 rather than H271 plays an important role in positioning the first substrate. In addition, the distance between the C_2 atom of DHE-ThDP and the S_6 atom of the lipoyl group (r_{c2-s6} for all structures here) is 3.46 Å in IM3_H128A. The substrate still locates at the favorable position for the ligation of DHE-ThDP and the lipoyl group, which indicates that His128 plays minor role in positioning lipoyl. However, in the H271A mutant, r_{c2-s6} is lengthened to 4.99 Å. Therefore, one can deduce that the low activity of the H271A mutant may be caused by the influence of the "open−close" transitions of the E1 subunit active-site loops, as suggested in previous studies,[27] and the mutated Ala271 that orients the lipoyl group in the unfavorable position.

■ CONCLUSIONS

In this article, the catalytic mechanism of the E1 subunit of the pyruvate dehydrogenase multienzyme complex has been investigated using DFT. Four possible pathways with different general acid/base catalysts in the decarboxylation and reductive acylation processes were considered. By calculating the reaction pathway of the H128A mutant and the pK_a value of ionizable residues, residue His271 is suggested to be in its deprotonated form during the reaction. The most possible reaction pathway, the detail of each elementary step, the energetics of the whole catalytic cycle, and the roles of some key residues were determined. Our calculation results indicated that Path-1A is the most favorable pathway, where the 4′-amino pyrimidine of ThDP and residue His128 act as the acid/base catalysts in the decarboxylation and reductive acylation processes, respectively. Except for the formation of CO_2, each C−C or C−S bond formation or cleavage process is always accompanied by a proton transfer. More importantly, the C−C or C−S bond formation always occurs prior to the proton transfer, and the C−C bond cleavage always occurs after proton transfer, suggesting that C−C or C−S bond ligation promotes the proton transfer and that proton transfer facilitates C−C bond cleavage. On the basis of our models, the liberation of CO_2 is calculated to be rate-limiting for the overall reaction with an energy barrier of 13.57 kcal/mol. The decarboxylation process is endothermic by 5.32 kcal/mol, whereas the reductive acylation process is exothermic with a value of 5.74 kcal/mol. Our calculations on the reaction pathways with different protonation states of His271 and His128 reveal that the protonation states of the surrounding residues can greatly influence the reaction. By optimizing the structure of the pyruvate-bound and lipoyl-bound mutants, residues His128 and His271 are proved to play roles in positioning the first substrate pyruvate and the second substrate lipoyl group of the E2 subunit lipoly domain, respectively. In addition, by comparing the energy barriers of each step using a polarizable-continuum model (PCM), we found that the surrounding environment is crucial for this enzymatic reaction. Our results may provide useful information for the design of novel drugs that have high efficiency and for the redesign of enzyme activities for biocatalytic applications.

dx.doi.org/10.1021/bi400577f | *Biochemistry* 2013, 52, 8079−8093

■ ASSOCIATED CONTENT

Supporting Information

Characteristic torsion angles Φ_T and Φ_P for the orientation of ThDP rings as well as the entropy changes of all species in the four reaction pathways. Optimized geometries of all species involved in the first step of the PDHc E1 subunit catalytic reaction with residue Glu59. Optimized geometries and energy profile of reductive acylation process catalyzed by the H128A mutant. Calculated IRC profiles of Path-1A. Energy profiles of Path-1A in the gas and solvent phases (PCM, ε = 80). This material is available free of charge via the Internet at http://pubs.acs.org.

■ AUTHOR INFORMATION

Corresponding Author

*Tel.: +86 531 883 655 76; Fax: +86 531 885 644 64; E-mail: yongjunliu_1@sdu.edu.cn.

Funding

This work was supported by the Natural Science Foundation of China (21373125 and 21173129).

Notes

The authors declare no competing financial interest.

■ ABBREVIATIONS USED

PDHc, pyruvate dehydrogenase multienzyme complex; OADH, 2-oxo acid dehydrogenase; CoA, coenzyme A; NAD^+, nicotinamide adenine dinucleotide; ThDP: thiamine diphosphate; DHE-ThDP, 1,2-dihydroxylethyl-ThDP; PSBD, peripheral subunit binding domain; TCA, tricarboxylic acid

■ REFERENCES

(1) de Kok, A., Hengeveld, A. F., Martin, A., and Westphal, A. H. (1998) The pyruvate dehydrogenase multienzyme complex from Gram-negative bacteria. *Biochim. Biophys. Acta 1385*, 353−366.

(2) Rochea, T. E., and Reed, L. J. (1972) Function of the nonidentical subunits of mammalian pyruvate dehydrogenase. *Biochem. Biophys. Res. Commun. 48*, 840−846.

(3) Bates, D. L., Danson, M. J., Hale, G., Hopper, E. A., and Perham, R. N. (1977) Self-assembly and catalytic activity of the pyruvate dehydrogenase multienzyme complex of *Escherichia coli*. *Nature 268*, 313−316.

(4) Ghosh, R., Guest, J. R., and Jeyaseelan, K. (1981) Regulatory properties of the pyruvate dehydrogenase complex of *Pseudomonas aeruginosa*. *Biochim. Biophys. Acta 658*, 232−237.

(5) Perham, R. N. (2000) Swinging arms and swinging domains in multifunctional enzymes: Catalytic machines for multistep reactions. *Annu. Rev. Biochem. 69*, 961−1004.

(6) Berg, A., and de Kok, A. (1997) 2-Oxo acid dehydrogenase multienzyme complexes. The central role of the lipoyl domain. *Biol. Chem. 378*, 617−634.

(7) Patel, M. S., and Harris, R. A. (1995) Alpha-keto acid dehydrogenase complexes: Nutrient control, gene regulation and genetic defects. *J. Nutr. 125*, 1744−1745.

(8) Perham, R. N. (1991) Domains, motifs, and linkers in 2-oxo acid dehydrogenase multienzyme complexes: A paradigm in the design of a multifunctional protein. *Biochemistry 30*, 8501−8512.

(9) Schellenberger, A. (1998) Sixty years of thiamin diphosphate biochemistry. *Biochim. Biophys. Acta 1385*, 177−186.

(10) Oliver, R. M., and Reed, L. J. (1982) Multienzyme complexes. In *Electron Microscopy of Proteins* (Harris, J. R., Ed.) pp 1−48, Academic Press, London.

(11) Reed, L. J. (1974) Multienzyme complexes. *Acc. Chem. Res. 7*, 40−46.

(12) Lengyel, J. S., Stott, K. M., Wu, X., Brooks, B. R., Balbo, A., Schuck, P., Perham, R. N., Subramaniam, S., and Milne, J. L. (2008) Extended polypeptide linkers establish the spatial architecture of a pyruvate dehydrogenase multienzyme complex. *Structure 16*, 93−103.

(13) Perham, R. N., Duckworth, H. W., and Roberts, G. C. (1981) Mobility of polypeptide chain in the pyruvate dehydrogenase complex revealed by proton NMR. *Nature 292*, 474−477.

(14) Patel, M. S., and Korotchkina, L. G. (2003) The biochemistry of the pyruvate dehydrogenase complex. *Biochem. Mol. Biol. Educ. 31*, 5−15.

(15) Barnerias, C., Saudubray, J. M., Touati, G., De Lonlay, P., Dulac, O., Ponsot, G., Marsac, C., Brivet, M., and Desguerre, I. (2010) Pyruvate dehydrogenase complex deficiency: Four neurological phenotypes with differing pathogenesis. *Dev. Med. Child Neurol. 52*, e1−e9.

(16) Prasad, C., Rupar, T., and Prasad, A. N. (2011) Pyruvate dehydrogenase deficiency and epilepsy. *Brain Dev. 33*, 856−865.

(17) Wada, N., Matsuishi, T., Nonaka, M., Naito, E., and Yoshino, M. (2004) Pyruvate dehydrogenase E1α subunit deficiency in a female patient: Evidence of antenatal origin of brain damage and possible etiology of infantile spasms. *Brain Dev. 26*, 57−60.

(18) Stacpoole, P. W., Owen, R., and Flotte, T. R. (2003) The pyruvate dehydrogenase complex as a target for gene therapy. *Curr. Gene Ther. 3*, 239−245.

(19) Stacpoole, P. W. (2012) The pyruvate dehydrogenase complex as a therapeutic target for age-related diseases. *Aging Cell 11*, 371−377.

(20) Dahl, H. M. (1995) Pyruvate dehydrogenase E1α deficiency: Males and females differ yet again. *Am. J. Hum. Genet. 56*, 553−557.

(21) Lissens, W., De Meirleir, L., Seneca, S., Liebaers, I., Brown, G. K., Brown, R. M., Ito, M., Naito, E., Kuroda, Y., Kerr, D. S., Wexler, I. D., Patel, M. S., Robinson, B. H., and Seyda, A. (2000) Mutations in the X-linked pyruvate dehydrogenase (E1) α subunit gene (PDHA1) in patients with a pyruvate dehydrogenase complex deficiency. *Hum. Mutat. 15*, 209−219.

(22) Brown, G. K. (1992) Pyruvate dehydrogenase E1α deficiency. *J. Inherited Metab. Dis. 15*, 625−633.

(23) Pei, X. Y., Titman, C. M., Frank, R. A. W., Leeper, F. J., and Luisi, B. F. (2008) Snapshots of catalysis in the E1 subunit of the pyruvate dehydrogenase multienzyme complex. *Structure 16*, 1860−1872.

(24) Fries, M., Jung, H., and Perham, R. N. (2003) Reaction mechanism of the heterotetrameric ($\alpha_2\beta_2$) E1 component of 2-oxo acid dehydrogenase multienzyme complexes. *Biochemistry 42*, 6996−7002.

(25) Kleiger, G., Perry, J., and Eisenberg, D. (2001) 3D structure and significance of the GΦXXG helix packing motif in tetramers of the E1β subunit of pyruvate dehydrogenase from the Archeon *Pyrobaculum aerophilum*. *Biochemistry 40*, 14484−14492.

(26) Arjunan, P., Nemeria, N., Brunskill, A., Chandrasekhar, K., Sax, M., Yan, Y., Jordan, F., Guest, J. R., and Furey, W. (2002) Structure of the pyruvate dehydrogenase multienzyme complex E1 component from *Escherichia coli* at 1.85 Å resolution. *Biochemistry 41*, 5213−5221.

(27) Frank, R. A. W., Pratap, J. V., Pei, X. Y., Perham, R. N., and Luisi, B. F. (2005) The molecular origins of specificity in the assembly of a multienzyme complex. *Structure 13*, 1119−1130.

(28) Muller, Y. A., Lindqvist, Y., Furey, W., Schulz, G. E., Jordan, F., and Schneider, G. (1993) A thiamin diphosphate binding fold revealed by comparison of the crystal structures of transketolase, pyruvate oxidase and pyruvate decarboxylase. *Structure 1*, 95−103.

(29) Frank, R. A., Leeper, F. J., and Luisi, B. F. (2007) Structure, mechanism and catalytic duality of thiamine-dependent enzymes. *Cell. Mol. Life Sci. 64*, 892−905.

(30) Liu, S., Gong, X., Yan, X., Peng, T., Baker, J. C., Li, L., Robben, P. M., Ravindran, S., Andersson, L. A., Cole, A. B., and Roche, T. E. (2001) Reaction mechanism for mammalian pyruvate dehydrogenase using natural lipoyl domain substrates. *Arch. Biochem. Biophys. 386*, 123−135.

(31) Pan, K., and Jordan, F. (1998) D,L-S-Methyllipoic acid methyl ester, a kinetically viable model for S-protonated lipoic acid as the oxidizing agent in reductive acyl transfers catalyzed by the 2-oxoacid dehydrogenase multienzyme complexes. *Biochemistry 37*, 1357−1364.

(32) Fries, M., Chauhan, H. J., Domingo, G. J., Jung, H., and Perham, R. N. (2003) Site-directed mutagenesis of a loop at the active site of E1 ($\alpha_2\beta_2$) of the pyruvate dehydrogenase complex. *Eur. J. Biochem. 270*, 861−870.
(33) Nemeria, N., Arjunan, P., Brunskill, A., Sheibani, F., Wei, W., Yan, Y., Zhang, S., Jordan, F., and Furey, W. (2002) Histidine 407, a phantom residue in the E1 subunit of the *Escherichia coli* pyruvate dehydrogenase complex, activates reductive acetylation of lipoamide on the E2 Subunit. An explanation for conservation of active sites between the E1 subunit and transketolase. *Biochemistry 41*, 15459−15467.
(34) Seifert, F., Ciszak, E., Korotchkina, L., Golbik, R., Spinka, M., Dominiak, P., Sidhu, S., Brauer, J., Patel, M. S., and Tittmann, K. (2007) Phosphorylation of Serine 264 impedes active site accessibility in the E1 component of the human pyruvate dehydrogenase multienzyme complex. *Biochemistry 46*, 6277−6287.
(35) Frank, R. A., Titman, C. M., Pratap, J. V., Luisi, B. F., and Perham, R. N. (2004) A molecular switch and proton wire synchronize the active sites in thiamine enzymes. *Science 306*, 872−876.
(36) Nemeria, N. S., Arjunan, P., Chandrasekhar, K., Mossad, M., Tittmann, K., Furey, W., and Jordan, F. (2010) Communication between thiamin cofactors in the *Escherichia coli* pyruvate dehydrogenase complex E1 component active centers. *J. Biol. Chem. 285*, 11197−11209.
(37) Arjunan, P., Sax, M., Brunskill, A., Chandrasekhar, K., Nemeria, N., Zhang, S., Jordan, F., and Furey, W. (2006) A thiamin-bound, pre-decarboxylation reaction intermediate analogue in the pyruvate dehydrogenase E1 subunit induces large scale disorder-to-order transformations in the enzyme and reveals novel structural features in the covalently bound adduct. *J. Biol. Chem. 281*, 15296−15303.
(38) Jordan, F., and Nemeria, N. S. (2005) Experimental observation of thiamin diphosphate-bound intermediates on enzymes and mechanistic information derived from these observations. *Bioorg. Chem. 33*, 190−215.
(39) Nemeria, N., Korotchkina, L., McLeish, M. J., Kenyon, G. L., Patel, M. S., and Jordan, F. (2007) Elucidation of the chemistry of enzyme-bound thiamine diphosphate prior to substrate binding: Defining internal equilibria among tautomeric and ionization states. *Biochemistry 46*, 10739−10744.
(40) Nemeria, N., Chakraborty, S., Baykal, A., Korotchkina, L. G., Patel, M. S., and Jordan, F. (2007) The 1′,4′-iminopyrimidine tautomer of thiamin diphosphate is poised for catalysis in asymmetric active centers on enzymes. *Proc. Natl. Acad. Sci. U.S.A. 104*, 78−82.
(41) Wang, J. Y., Dong, H., Li, S. H., and He, H. W. (2005) Theoretical study toward understanding the catalytic mechanism of pyruvate decarboxylase. *J. Phys. Chem. B 109*, 18664−18672.
(42) Hou, Q., Gao, J., Liu, Y., and Liu, C. (2012) A QM/MM study on the catalytic mechanism of pyruvate decarboxylase. *Theor. Chem. Acc. 131*, 1280.
(43) Friedemann, R., Tittmann, K., Golbik, R., and Hübner, G. (2009) DFT and MP2 studies on the C2-C2 bond cleavage in thiamin catalysis. *J. Mol. Catal. B 61*, 36−38.
(44) Assary, R. S., and Broadbelt, L. J. (2011) Computatinal screening of novel thiamine-catalyzed decarboxylation reactions of 2-keto acids. *Bioprocess Biosyst. Eng. 34*, 375−388.
(45) Jaña, G., Jiménez, V., Villà-Freixa, J., Prat-Resina, X., Delgado, E., and Alderete, J. B. (2011) A QM/MM study on the last two steps of the catalytic cycle of acetohydroxyacid synthase. *Comput. Theor. Chem. 96*, 159−166.
(46) Jaña, G., Jiménez, V., Villà-Freixa, J., Prat-Resina, X., Delgado, E., and Alderete, J. B. (2010) Computational study on the carboligation reaction of acetohydroxyacid synthase: New approach on the role of the HEThDP-intermediate. *Proteins 78*, 1774−1788.
(47) Xiong, Y., Liu, J., Yang, G. F., and Zhan, C. G. (2010) Computational determination of fundamental pathway and activation barriers for acetohydroxyacid synthase-catalyzed condensation reactions of α-keto acids. *J. Comput. Chem. 31*, 1592−1602.
(48) Sheng, X., Liu, Y., and Liu, C. (2013) Theoretical studies on the common catalytic mechanism of transketolase by using simplified model. *J. Mol. Graphics Modell. 39*, 23−28.
(49) Wang, J. Y., and Li, S. H. (2006) Theoretical study toward understanding the catalytic mechanism of pyruvate dehydrogenase multienzyme complex E1 component. *J. Theor. Comput. Chem. 5*, 447−459.
(50) Becke, A. D. (1988) Density-functional exchange-energy approximation with correct asymptotic behavior. *Phys. Rev. A 38*, 3098−3100.
(51) Lee, C., Yang, W., and Parr, R. G. (1998) Development of the Colle−Salvetti correlation-energy formula into a functional of the electron density. *Phys. Rev. B 37*, 785−789.
(52) Acosta-Silva, C., Bertran, J., Branchadell, V., and Oliva, A. (2012) Quantum-mechanical study on the mechanism of peptide bond formation in the ribosome. *J. Am. Chem. Soc. 134*, 5817−5831.
(53) Lind, M. E. S., and Himo, F. (2013) Quantum chemistry as a tool in asymmetric biocatalysis: Limonene epoxide hydrolase test case. *Angew. Chem., Int. Ed. 52*, 4563−4567.
(54) Mayilmurugan, R., Harum, B. N., Volpe, M., Sax, A. F., Palaniandavar, M., and Mösch-Zanetti, N. C. (2011) Mechanistic insight into the reactivity of oxotransferases by novel asymmetric dioxomolybdenum(VI) model complexes. *Chem.—Eur. J. 17*, 704−713.
(55) Miłaczewska, A., Broclawik, E., and Borowski, T. (2013) On the catalytic mechanism of (S)-2-hydroxypropylphosphonic acid epoxidase (HppE): A hybrid DFT study. *Chem.—Eur. J. 19*, 771−781.
(56) Marino, T., Russo, N., and Toscano, M. (2013) Catalytic mechanism of the arylsulfatase promiscuous enzyme from *Pseudomonas aeruginosa*. *Chem.—Eur. J. 19*, 2185−2192.
(57) Kamachi, T., Nakayama, T., Shitamichi, O., Jitsumori, K., Kurihara, T., Esaki, N., and Yoshizawa, K. (2009) The catalytic mechanism of fluoroacetate dehalogenase: A computational exploration of biological dehalogenation. *Chem.—Eur. J. 15*, 7394−7403.
(58) Jun, X., Zhang, J. Z. H., and Xiang, Y. (2012) Ab initio QM/MM free energy simulations of peptide bond formation in the ribosome support an eight-membered ring reaction mechanism. *J. Am. Chem. Soc. 134*, 16424−16429.
(59) López-Canut, V., Ruiz-Pernía, J. J., Castillo, R., Moliner, V., and Tuñón, I. (2012) Hydrolysis of phosphotriesters: A theoretical analysis of the enzymatic and solution mechanisms. *Chem.—Eur. J. 18*, 9612−9621.
(60) Kern, D., Kern, G., Neef, H., Tittmann, K., Killenberg-Jabs, M., Wikner, C., Schneider, G., and Hubner, G. (1997) How thiamine diphosphate is activated in enzymes. *Science 275*, 67−70.
(61) Tittmann, K., Mesch, K., Pohl, M., and Hübner, G. (1998) Activation of thiamine diphosphate in pyruvate decarboxylase from *Zymomonas mobilis*. *FEBS Lett. 441*, 404−406.
(62) Bar-Ilan, A., Balan, V., Tittmann, K., Golbik, R., Vyazmensky, M., Hübner, G., Barak, Z., and Chipman, D. M. (2001) Binding and activation of thiamin diphosphate in acetohydroxyacid synthase. *Biochemitry 40*, 11946−11954.
(63) Fang, R., Nixon, P. F., and Duggleby, R. G. (1998) Identification of the catalytic glutamate in the E1 component of human pyruvate dehydrogenase. *FEBS Lett. 437*, 273−277.
(64) Shaanan, B., and Chipman, D. M. (2009) Reaction mechanism of thiamin diphosphate enzymes: New insights into the role of a conserved glutamate residue. *FEBS J. 276*, 2447−2453.
(65) Sondergaard, C. R., Olsson, M. H. M., Rostkowski, M., and Jensen, J. H. (2011) Improved treatment of ligands and coupling effects in empirical calculation and rationalization of pKa values. *J. Chem. Theory Comput. 7*, 2284−2295.
(66) Olsson, M. H. M., Sondergard, C. R., Rostkowski, M., and Jensen, J. H. (2011) PROPKA3: Consistent treatment of internal and surface residues in empirical pK_a predictions. *J. Chem. Theory Comput. 7*, 525−537.
(67) Frisch, M. J., Trucks, G. W., Schlegel, H. B., Scuseria, G. E., Robb, M. A., Cheeseman, J. R., Scalmani, G., Barone, V., Mennucci, B., Petersson, G. A., Nakatsuji, H., Caricato, M., Li, X., Hratchian, H. P.,

Izmaylov, A. F., Bloino, J., Zheng, G., Sonnenberg, J. L., Hada, M., Ehara, M., Toyota, K., Fukuda, R., Hasegawa, J., Ishida, M., Nakajima, T., Honda, Y., Kitao, O., Nakai, H., Vreven, T., Montgomery, J. A., Jr., Peralta, J. E., Ogliaro, F., Bearpark, M., Heyd, J. J., Brothers, E., Kudin, K. N., Staroverov, V. N., Keith, T., Kobayashi, R., Normand, J., Raghavachari, K., Rendell, A., Burant, J. C., Iyengar, S. S., Tomasi, J., Cossi, M., Rega, N., Millam, J. M., Klene, M., Knox, J. E., Cross, J. B., Bakken, V., Adamo, C., Jaramillo, J., Gomperts, R., Stratmann, R. E., Yazyev, O., Austin, A. J., Cammi, R., Pomelli, C., Ochterski, J. W., Martin, R. L., Morokuma, K., Zakrzewski, V. G., Voth, G. A., Salvador, P., Dannenberg, J. J., Dapprich, S., Daniels, A. D., Farkas, O., Foresman, J. B., Ortiz, J. V., Cioslowski, J., and Fox, D. J. (2010) *Gaussian 09, Revision B.01*, Gaussian, Inc., Wallingford, CT.

(68) Barone, V., Cossi, M., and Tomasi, J. (1998) Geometry optimization of molecular structures in solution by the polarizable continuum model. *J. Comput. Chem. 19*, 404−417.

(69) Tomasi, J., and Persico, M. (1994) Molecular interactions in solution: An overview of methods based on continuous distributions of the solvent. *Chem. Rev. 94*, 2027−2094.

(70) Robinet, J. J., Cho, K. B., and Gauld, J. W. (2008) A density functional theory investigation on the mechanism of the second half-reaction of nitric oxide synthase. *J. Am. Chem. Soc. 130*, 3328−3334.

(71) Liao, R. J., Ding, W. J., Yu, J. G., Fang, W. H., and Liu, R. Z. (2008) Theoretical studies on pyridoxal 5′-phosphate-dependent transamination of α-amino acids. *J. Comput. Chem. 29*, 1919−1929.

(72) Gonzalez, C., and Schlegel, H. B. (1989) An improved algorithm for reaction path following. *J. Chem. Phys. 90*, 2154−2161.

(73) Gonzalez, C., and Schlegel, H. B. (1990) Reaction path following in mass-weighted internal coordinates. *J. Phys. Chem. 94*, 5523−5527.

(74) Muller, Y. A., Lindqvist, Y., Furey, W., Schuza, G. E., Jordan, F., and Schneider, G. (1993) A thiamin diphosphate binding old revealed by comparison of the crystal structures of transketolase pyruvate oxidase and pyruvate decarboxylase. *Structure 1*, 95−103.

(75) Muller, Y. A., and Schulz, G. E. (1993) Structure of the thiamine- and flavin-dependent enzyme pyruvate oxidase. *Science 259*, 965−967.

(76) Asztalos, P., Parthier, C., Golbik, R., Kleinschmidt, M., Hübner, G., Weiss, M. S., Friedemann, R., Wille, G., and Tittmann, K. (2007) Strain and near attack conformers in enzymic thia min catalysis: X-ray crystallographic snapshots of bacterial transketolase in covalent complex with donor ketoses cylulose 5-phosphate and fructose 6-phosphate, and in noncovalent complex with acceptor aldose ribose 5-phosphate. *Biochemistry 46*, 12037−12052.

(77) Mitschke, L., Parthier, C., Schröeder-Tittmann, K., Coy, J., Lüdtke, S., and Tittmann, K. (2010) The crystal structure of human transketolase and new insights into its mode of action. *J. Biol. Chem. 285*, 31559−31570.

(78) Danson, M. J., Fersht, A. R., and Perham, R. N. (1978) Rapid intramolecular coupling of active sites in the pyruvate dehydrogenase complex of *Escherichia coli*: Mechanism for rate enhancement in a multimeric structure. *Proc. Natl. Acad. Sci. U.S.A. 75*, 5386−5390.

(79) Cate, R. L., Roche, T. E., and Davis, L. C. (1980) Rapid intersite transfer of acetyl groups and movement of pyruvate dehydrogenase component in the kidney pyruvate dehydrogenase complex. *J. Biol. Chem. 255*, 7556−7562.

(80) Berg, A., Westphal, A. H., Bosma, H. J., and de Kok, A. (1998) Kinetics and specificity of reductive acylation of wild-type and mutated lipoyl domains of 2-oxo-acid dehydrogenase complexes from *Azotobacter Vinelandii*. *Eur. J. Biochem. 252*, 45−50.